Spring persistence, transition and resurgence of El Niño

Sang-Ki Lee[1,2], Pedro N. DiNezio[3], Eui-Seok Chung[4], Sang-Wook Yeh[5], Andrew T. Wittenberg[6], and Chunzai Wang[2]

[1]Cooperative Institute for Marine and Atmospheric Studies, University of Miami, Miami, Florida

[2]NOAA Atlantic Oceanographic and Meteorological Laboratory, Miami, Florida

[3]Department of Oceanography, School of Ocean and Earth Science and Technology, University of Hawai'i at Mānoa, Honolulu, Hawaii

[4]Rosenstiel School of Marine and Atmospheric Sciences, University of Miami, Miami, Florida

[5]Department of Marine Sciences and Convergent Technology, Hanyang University, Ansan, Korea

[6]NOAA Geophysical Fluid Dynamics Laboratory, Princeton, New Jersey

Revised for Geophysical Research Letters

November 2014

Corresponding author address: Dr. Sang-Ki Lee, CIMAS, University of Miami, 4600 Rickenbacker Causeway, Miami, FL 33149, USA. E-mail: Sang-Ki.Lee@noaa.gov.

Abstract

We present a systematic exploration of differences in the spatio-temporal sea surface temperature (SST) evolution along the equatorial Pacific among observed El Niño events. This inter-El Niño variability is captured by two leading orthogonal modes, which explain more than 60% of the inter-event variance. The first mode illustrates the extent to which warm SST anomalies (SSTAs) in the eastern tropical Pacific (EP) persist into the boreal spring after the peak of El Niño. Our analysis suggests that a strong El Niño event tends to persist into the boreal spring in the EP, whereas a weak El Niño favors a rapid development of cold SSTAs in the EP shortly after its peak. The second mode captures the transition and resurgence of El Niño in the following year. An early-onset El Niño tends to favor a transition to La Niña, whereas a late-onset El Niño tends to persist long enough to produce another El Niño event. The spatio-temporal evolution of several El Niño events during 1949-2013 can be efficiently summarized in terms of these two modes, which are not mutually exclusive, but exhibit distinctive coupled atmosphere-ocean dynamics.

1. Introduction

Although it has been long recognized that more than one degree of freedom is needed to describe El Niño–Southern Oscillation (ENSO) [*Trenberth and Stepaniak*, 2001], inter-ENSO variability (or ENSO diversity) has received renewed attention in recent years. As summarized in two recent review articles [*Capotondi et al*., 2015; *Yeh et al*., 2014], there is a continuum of ENSO spatial patterns of anomalous sea surface temperature (SST), thermocline depth, zonal currents and atmospheric convection. At two extremes of this continuum are the "El Niño Modoki" (also referred to as "Central Pacific El Niño", "Dateline El Niño" and "Warm Pool El Niño" in the literature), which has its peak SST anomalies (SSTAs) in the central tropical Pacific (CP); and the "conventional El Niño" which typically has its peak SSTAs in the eastern tropical Pacific (EP). Since the zonal SST gradient is relatively strong and the thermocline is relatively deep in the CP, the growth of the "El Niño Modoki" relies more on the zonal advection feedback than the thermocline feedback [*Jin and An*, 1999; *Kug et al*., 2010]. Several studies have also noted that "El Niño Modoki" is more associated with surface heat flux variability as opposed to ocean dynamics [e.g., *Yu et al*., 2010].

ENSO SSTAs tend to peak during boreal winter [*Rasmusson and Carpenter*, 1982]. Thus, the great majority of recent studies on ENSO diversity have focused on the different spatial patterns of ENSO SSTAs during the peak phase in December to February (DJF [0,+1]); hereafter any month in an ENSO onset year is identified by the suffix (0) whereas any month in an ENSO decay year by the suffix (+1). In contrast, inter-event differences in the temporal evolution of ENSO have received much less attention [e.g., *Lengaigne et al*., 2006; *McPhaden and Zhang*, 2009; *Yu and Kim*, 2010; *Takahashi et al*., 2011; *Choi et al*., 2013; *Dommenget et al*, 2013; *McGregor et al*., 2013; *DiNezio and Deser*, 2014]. However, the onset and decay phases of

ENSO typically occurring in boreal spring and summer also play very important roles in forcing climate variability around the globe associated with the East Asian monsoon, tropical cyclones, terrestrial rainfalls and extra-tropical extreme weather events [e.g., *Wu and Wang*, 2002; *Camargo and Sobel*, 2005; *Larson et al*., 2012; *Lee et al*., 2013; 2014; *Wang and Wang*, 2013].

Our main goal in this study is to identify and explain the spatio-temporal evolution of inter-El Niño variability in the tropical Pacific for the entire lifespan of El Niño from onset to decay. To achieve this, here we present an objective methodology to identify two leading orthogonal modes of inter-El Niño variability (section 2 and 3). We also present possible mechanisms leading to the two orthogonal modes (section 4 and 5). Then, we discuss the occurrence of the two modes in observed El Niño events and present rotated orthogonal modes to better characterize several observed El Niño events (section 6).

2. Data and Methods

We explore the spatio-temporal evolution of observed El Niño events in the following datasets. The Extended Reconstructed Sea Surface Temperature version 3b (ERSST3), an in situ analysis of global monthly SST on a 2° longitude by 2° latitude grid [*Smith et al*., 2008], is used to compute SSTAs in the equatorial Pacific for the period of 1949-2013. Two reanalysis products are also used to explore the coupled atmosphere-ocean processes involved with the two orthogonal modes. The Simple Ocean Data Assimilation (SODA) ocean reanalysis [*Giese and Ray*, 2011] is used to derive the depth of 20ºC isotherm (D20), a proxy for the depth of thermocline. The 20th Century Reanalysis (20CR) [*Compo et al*., 2011] is used to derive surface wind stress fields.

We identify 21 El Niño events during the period of 1949-2013 based on the threshold that the 3-month averaged SSTAs in Niño 3.4 (120°W–170°W and 5°S–5°N) exceed 0.5°C for a minimum of five consecutive months, following the definition used at NCEP. There are a few multi-year El Niño events during the study period. They are treated here as multiple El Niño events. For instance, the El Niño that started in the summer of 1986 and continued until the early spring of 1988 is treated as two consecutive El Niño events; that is, the onset and decay of the 1986–1987 El Niño followed by the onset and decay of the 1987–1988 El Niño. See Figure S1 in the supporting information for details on the individual events included in this analysis.

Next, we construct longitude-time maps of equatorial Pacific SSTAs (averaged between the 5ºS and 5ºN latitude bands) for each individual event. The time and longitude axes span from January of the onset year to December of the decay year, and the entire equatorial Pacific (120ºE - 80ºW), respectively. We then perform an Empirical Orthogonal Function (EOF) analysis of these 21 longitude-time maps of equatorial Pacific SSTAs in order to isolate the preferred spatio-temporal modes of inter-El Niño variability. Note that the resulting principal components (PCs) are associated with each individual El Niño event.

By using EOF modes (EOFs) to explore the inter-El Niño variability, we do not mean to imply that there is any multi-modality in the distribution of El Niño events, nor that El Niño events tend to cluster around specific discrete types. The EOFs simply represent a linearly independent set of longitude-time structures that capture the maximum amount of inter-event variance. As such, they should serve as an efficient basis for describing the continuum of El Niño evolutions.

3. Two Leading Modes of Inter-El Niño Variability

The two leading EOFs are shown in Figure 1b and c along with the composite mean (CM) of the tropical Pacific El Niño SSTAs in Figure 1a. The first and second EOFs represent 34.4% and 27.6% of the total inter-El Niño variance, respectively, while the third EOF represents only 9.6% of the total inter-El Niño variance (not shown). Overall, the amplitude of inter-El Niño variability is largest in the decay year after the peak season.

The first EOF mode (Figure 1b) mainly illustrates inter-event variability of SSTAs in the EP during April, May and June of the decay year (AMJ [+1]) as also evident in Figure S2a. As shown in Figure S2b, the first EOF mode is highly correlated with the Niño 3.4 index for the peak season (r = 0.74; significant above 99.9% level). This means that a strong El Niño event tends to persist into the boreal spring in the EP. In contrast, a weak El Niño event favors a rapid development of cold SSTAs in the EP after the peak season and a transition to La Niña. Three El Niño events (1982-1983, 1991-1992 and 1997-1998) are examples of the former (i.e., strong and persistent). Five other El Niño events (1953-1954, 1963-1964, 1969-1970, 1977-1978 and 1987-1988) fit well with the latter (i.e., weak and early-terminating).

The second EOF mode (Figure 1c) captures inter-event variability in the central and eastern tropical Pacific during October, November and December of the decay year (OND [+1]) as also evident in Figure S2c. Thus, it mainly describes whether El Niño will return for a consecutive year or transition into La Niña. This mode is also well correlated with the SSTAs in Niño 3.4 for DJF (0,+1), but not as strong as the correlation with the first mode (r = 0.49; significant at 95% level; not shown). This means that while a strong (weak) El Niño event does favor a following La Niña (El Niño) event, the peak season strength of El Niño may not be the dictating factor.

Interestingly, the second EOF mode is better correlated with the SSTAs in Niño 3 during AMJ (0) as shown in Figure S2d (r = 0.78; significant above 99.9% level). In other words, if the

EP warms early in boreal spring and summer to produce an early onset of El Niño, that El Niño event tends to favor a transition to La Niña as it dissipates. On the other hand, if the EP warms late in boreal fall and winter to produce a late-onset of El Niño, it tends to favor a subsequent resurgence of the El Niño. This conjecture is indeed supported by our further analysis to be discussed in section 5. Four El Niño events (1972-1973, 1982-1983, 1987-1988 and 1997-1998) can be considered as the former (i.e., early-onset and transitioning). Only two El Niño events (1968-1969 and 1986-1987) fit with the latter (i.e., late-onset and resurgent).

4. Spring Persistence of El Niño

To better understand the atmosphere-ocean dynamics associated with the first EOF mode, here we explore the longitude-time maps of anomalous SST, D20, and surface wind stress vectors regressed onto PC1. The first EOF mode describes a continuum of El Niño events ranging from those that persist well into boreal spring (PC1 = 1) to those that terminate early and transition to La Niña (PC1 = -1). We analyze both the persistent and early-terminating cases by adding EOF1 to CM and subtracting EOF1 from CM, respectively.

The persisting El Niño case (CM+EOF1) exhibits much stronger SSTAs and deeper thermocline anomalies over the EP during the peak season (Figure 2b) in comparison to CM (Figure 2a). While the climatological SSTs in the EP are generally quite cold near the end of the calendar year (Figure S3), sufficiently strong warm SSTAs in the EP during this time can favor atmospheric deep convection (see Figure S4b) and thus strongly reduce the equatorial easterly trade winds in the CP [*Hoerling et al*., 1997; *Jin et al*., 2003; *Lengaigne and Vecchi*, 2009]. Thus, as illustrated in Figure 2b, the thermocline in the EP further deepens and helps maintain the warm SSTAs in the EP throughout the boreal spring during which the warmer climatological

SSTs in the EP also help sustain deep convection; thus, the Bjerknes feedback remains active [e.g., *Lengaigne and Vecchi*, 2009].

During the second half of the onset year, due to the massive reduction of the easterlies, the thermocline shoals in the western tropical Pacific, and then gradually propagates toward the east in accordance with the behavior of a slow “SST mode”- slowly propagating anomalies whose time scale is set by coupled air-sea interactions, rather than by fast ocean wave dynamics [*Neelin*, 1991; *Wang and Weisberg*, 1996]. The transition to La Niña, however, is presumably suppressed by reduced entrainment of subsurface waters into the mixed layer due to a prolonged weakening of the trade winds.

Consistent with our interpretation of CM+EOF1, the two extreme El Niño events, namely the 1982-1983 and 1997-1998 events, persisted into the boreal spring after the peak season. For these two events, the peak season total SSTs in the EP exceeded the present-day threshold value for deep convection [*Lengaigne and Vecchi*, 2009; *Vecchi and Harrison*, 2006; *Vecchi*, 2006]. However, both of these El Niño events transitioned to La Niña events, unlike the strong and persistent case described by CM+EOF1. This suggests that the 1982-1983 and 1997-1998 events cannot be solely described by CM+EOF1.

As shown in Figure 2c, the early-terminating case (CM-EOF1) describes a weak El Niño that transitions to a La Niña event. This case is characterized by a rapid development of cold SSTAs in the EP shortly after the peak season. Since the climatological SSTs in the EP are quite cold in boreal winter, it is unlikely that a weak El Niño can induce deep convection in the EP during the peak season (Figure S3). Therefore, deep convection anomalies are much stronger in the CP than in the EP (see Figure S4c). This in turn induces easterly wind anomalies converging to the CP from the east; thus, the thermocline shoals in the far eastern tropical Pacific, and then cold

SSTAs develop in the EP shortly after the peak season. Since the climatological SSTs in the EP are warmest in boreal spring (Figure S3), the cold SSTAs in the EP could inhibit atmospheric convection (see Figure S4c) and thus reinforce the easterly winds. Therefore, a positive atmosphere-ocean feedback may kick in to further increase the easterly winds, which in turn may further decrease the thermocline depth in the EP and maintain the cold SSTAs in the EP throughout the decay year (Figure 2c).

Unlike the strong and persistent El Niño case described by CM+EOF1, an onset of the weak and early-terminating El Niño case described by CM-EOF1 does not involve eastward propagating thermocline depth anomalies. Thus, this is more likely to be induced by the zonal advection feedback, which amplifies initial warm SSTAs in the CP generated either locally or remotely [e.g., *Vimont et al.*, 2001; *Yu et al.*, 2010; *Zhang et al.*, 2013].

5. Transition and Resurgence of El Niño

As shown in Figure 2d, CM+EOF2 describes an El Niño that transitions to a La Niña event (i.e., transitioning El Niño). An important feature to note is that the thermocline in the EP is already quite deep in the boreal spring of the onset year, suggesting an early onset of El Niño. Therefore, the SST and zonal wind stress anomalies are already robust in the boreal spring and early summer of the onset year.

Figure 2d suggests that the onset of La Niña during the decay year is in accordance with the slow SST mode. It appears that the early developments of SST and zonal wind stress anomalies in the boreal spring and summer of the onset year help produce a massive shoaling of the thermocline in the western tropical Pacific that in turn slowly penetrates toward the east in accordance with the slow SST mode. Additionally, in response to the seasonal evolution of solar insolation, the westerly anomalies shift southward during the peak season (not shown) and thus also contribute to the eastward propagation of elevated thermocline anomalies [*Lengaigne et al*. 2006; *McGregor et al*., 2013]. Accordingly, the thermocline shoals and produces the cold SSTAs in the CP during the boreal summer of the decay year. In turn, the easterly winds increase to the west of the cold SSTAs. This appears to activate a positive atmosphere-ocean feedback, leading to a robust onset of La Niña (see Figure 2d and S4d).

The atmosphere-ocean processes linked to the El Niño-to-La Niña transitions described by CM+EOF2 and CM-EOF1 appear to be entirely different. As discussed earlier, central to the weak El Niño case described by CM-EOF1 are the enhanced easterlies converging from the east toward the CP during and after the peak season, which in turn presumably instigate a positive air-sea feedback to produce and amplify the cold SSTAs in the EP. On the other hand, the robust development and slow eastward-penetration of the air-sea coupled anomalies are the key points for the development of La Niña in the early-onset El Niño case described by CM+EOF2.

As shown in Figure 2e (and Figure S4e), CM-EOF2 describes an El Niño event that persists long enough to produce another El Niño event (i.e., resurgent El Niño). In this case, the SST, thermocline depth and zonal wind stress anomalies remain quite weak in the boreal spring and summer of the onset year, producing a delayed onset of El Niño.

It appears that the late developments of the SST and zonal wind stress anomalies do not allow enough time prior to and during the peak season to produce a robust shoaling of the thermocline in the western tropical Pacific. Thus, the eastward propagating shoaling signal dissipates before passing the date line. As a result, the deepened thermocline in the EP dissipates extremely slowly.

The thermocline depth anomalies are quite small beyond the boreal spring of the decay year. Therefore, it is unlikely that the prolonged but weak depression of the thermocline maintains the warm SSTAs in the CP beyond the boreal spring of the decay year. This suggests that the persistent warm SSTAs in the CP during the second half of the decay year may be maintained by other mechanisms such as the zonal advection feedback or the atmosphere-ocean thermal feedback [*Dommenget*, 2010; *Clement et al*., 2011; *Zhang et al*., 2014].

6. Occurrences of the Two Leading Modes in Observed El Niño Events

Figure 3a shows the normalized PC1 and PC2 for all 21 El Niño events. As shown, some El Niño events are readily characterized by using one of the two EOFs of inter-El Niño variability. For instance, three El Niño events (1953-1954, 1963-1964 and 1969-1970) are clearly weak and early-terminating in the EP (CM-EOF1), whereas the 1972-1973 El Niño event is early-onset and transitioning (CM+EOF2).

However, for many El Niño events including most of the strongest ones, both EOFs of inter-El Niño variability are required to characterize them. For instance, the two extreme El Niños, the 1982-1983 and 1997-1998 events, are not only strong and persistent in the EP (CM+EOF1) but also transitioning (CM+EOF2). It is therefore a useful exercise to rotate the two EOFs to better align their axes with the observed El Niño events. Such a procedure was applied by *Takahashi et al*., [2011] to reinterpret “conventional El Niño” and “El Niño Modoki”. For instance, Figure 3b shows the 90º-rotated PCs for all 21 El Niño events. The corresponding rotated EOFs are shown in Figure 1c and d. As illustrated in Figure 4b and c, the first rotated EOF effectively describes the two extreme El Niños versus weak El Niños (e.g., 1958-1959 and 1977-1978 events). Similarly, as shown in Figure 4d and e, the second rotated EOF reasonably well describes early-onset, early-terminating and transitioning El Niños (e.g., 1987-1988 event) versus late-onset, persistent and resurgent El Niños (e.g., 1968-1969 and 1986-1987 events).

Some other El Niño events, such as the 1951-1952, 1957-1958, 1965-1966, 1994-1995, 2004-2005, 2006-2007 events, cannot be clearly classified using the two leading EOFs or the rotated EOFs. This suggests that the spatio-temporal evolution associated with inter-El Niño variability is, to a certain extent, stochastic, supporting the idea of an "El Niño continuum" [*Giese and Ray*, 2011; *Capotondi et al*., 2015].

7. Discussion

Additional analyses were performed to test if and how the two leading EOFs were affected by the SST dataset used and by the criteria for identifying El Niño. First, the Hadley Centre SST data set was used to repeat the inter-El Niño EOF analysis, finding two leading EOFs that are almost identical to those derived from ERSST3 (not shown). Four additional El Niños, the 1979-1980, 1990-1991, 1992-1993, 2001-2002, and 2003-2004 events, that are not included in this study but were considered elsewhere [e.g., *Yeh et al*., 2009], are included to repeat the inter-El Niño EOF analysis. In that analysis, the second EOF mode becomes the dominant mode (36.3%) while the first EOF mode becomes the second dominant mode (24.8%). However, the spatio-temporal structures of the two EOFs are almost unaltered (not shown). These results suggest that the two leading EOFs of inter-El Niño variability described in this study are robust features in the available observations. However, given the modulation of ENSO [*Wittenberg*, 2009; *Wittenberg et al*., 2014; *Vecchi and Wittenberg*, 2010; *DiNezio et al*., 2012; *Ogata et al*. 2013; *Karamperidou et al*. 2014], future studies should investigate whether the leading modes of inter-event variation change from epoch to epoch, how they interact with the background climatology of the tropical Pacific, and how they could respond to future climate change.

The persistence, transition, and resurgence aspects captured by the two leading EOFs of inter-El Niño variability are closely related to the emergent time scale and predictability of the ENSO phenomenon. Thus the mechanisms described here connect to a large body of earlier work on the time scale and predictability of ENSO, in which the zonal and meridional structure of the ENSO wind response, and the seasonal timing of stochastic westerly wind events in the west Pacific, were found to strongly affect the period, amplitude, and predictability of ENSO events [e.g., *Kirtman*, 1997; *An and Wang*, 2000; *Capotondi et al*. 2006; *Vecchi et al*. 2006; *Gebbie et al*. 2007; *Lim et al.,* 2009; *Larson and Kirtman*, 2014; *Lopez and Kirtman*, 2014]. The present study provides a concise framework for summarizing these effects across multiple El Niño events, which can be used to characterize and compare El Niño behavior.

This study suggests that the peak season strength of El Niño is a predictor for the spring persistence and that the onset timing of El Niño is a predictor for the transitioning and resurgent El Niño. Therefore, simulating the two EOFs realistically appears to be a prerequisite for a seasonal prediction model to predict the spring persistence, transition and resurgence of El Niño. The predictability of these aspects of the temporal evolution of El Niño needs to be explored in a perfect-model framework.

Finally, it is important to note that our results specific to inter-El Niño variability cannot be directly applied to inter-La Niña variability with reversed sign due to the El Niño-La Niña asymmetry in spatial and time evolution [Dommenget et al., 2013]. As shown in Figure S5, it appears that the first EOF mode of inter-La Niña variability describes a two-year La Niña transitioning to El Niño, and El Niño transitioning to a two-year La Niña. Given that severe weather events over the U.S. frequently occur during the onset and decay phases of La Niña [e.g., *Lee et al*., 2013; 2014], it would be useful to explore inter-La Niña variability in future studies.

Acknowledgments. We would like to thank two anonymous reviewers, Hosmay Lopez and Chris Meinen for their thoughtful suggestions. This work was supported by NOAA/CPO through its MAPP program [NA12OAR4310083] and by the base funding of NOAA/AOML. ERSST3, SODA and 20CR were, respectively, provided by NOAA/ESRL/PSD at http://www.esrl.noaa.gov/psd/, by NOAA NCDC at http://www.ncdc.noaa.gov, and by TAMU SODA research group at http://soda.tamu.edu/data.htm.

References

An, S.-I., and B. Wang (2000), Interdecadal change of the structure of the ENSO mode and its impact on the ENSO frequency, *J. Clim.*, *13*, 2044-2055.

Camargo, S. J., and A. Sobel (2005), Western North Pacific tropical cyclone intensity and ENSO, *J. Clim.*, *18*, 2996-3006.

Capotondi, A., A. Wittenberg, and S. Masina (2006) Spatial and temporal structure of tropical Pacific interannual variability in 20th century coupled simulations, *Ocean Model.*, *15*, 274-298. doi: 10.1016/j.ocemod.2006.02.004.

Capotondi, A. et al. (2015), Understanding ENSO diversity. *Bull. Amer. Meteor. Soc.*, In-press. doi: 10.1175/BAMS-D-13-00117.1

Choi, K.-Y., G. A. Vecchi, and A. T. Wittenberg (2013), ENSO transition, duration and amplitude asymmetries: Role of the nonlinear wind stress coupling in a conceptual model, *J. Clim.*, *26*, 9462-9476. doi: 10.1175/JCLI-D-13-00045.1.

Clement, A. C., P. DiNezio, and C. Deser (2011), Rethinking the ocean's role in the Southern Oscillation, *J. Clim.*, *24*, 4056–4072.

Compo, G. P. et al. (2011), The twentieth century reanalysis project, *Q. J. R. Meteorol. Soc.*, *137*, 1–28, doi:10.1002/qj.776.

DiNezio, P. N., B. P. Kirtman, A. C. Clement, S.-K. Lee, G. A. Vecchi, and A. Wittenberg (2012), Mean climate controls on the simulated response of ENSO to increasing greenhouse gases, *J. Clim.*, *25*, 7399-7420. doi: 10.1175/JCLI-D-11-00494.1

DiNezio, P. N., and C. Deser (2014), Nonlinear controls on the persistence of La Niña, *J. Clim.*, In-press.

Dommenget, D. (2010), A slab ocean El Niño, *Geophys. Res. Lett.*, *37*, L20701, doi:10.1029/2010GL044888.

Dommenget, D., T. Bayr, and C. Frauen (2013), Analysis of the non-linearity in the pattern and time evolution of El Niño southern oscillation, *Clim. Dyn*, *40*, 2825-2847.

Gebbie, G., I. Eisenman, A. Wittenberg, and E. Tziperman (2007), Modulation of westerly wind bursts by sea surface temperature: A semistochastic feedback for ENSO, *J. Atmos. Sci.*, *64*, 3281-3295. doi: 10.1175/JAS4029.1.

Giese, B. S., and S. Ray (2011), El Niño variability in simple ocean data assimilation (SODA), 1871–2008, *J. Geophys. Res.*, *116*, C02024, doi:10.1029/2010JC006695.

Hoerling, M. P., A. Kumar, and M. Zhong (1997), El Niño, La Niña, and the nonlinearity of their teleconnections, *J. Clim.*, *10*, 1769–1786.

Jin, F.-F., and S.-I. An (1999), Thermocline and zonal advective feedbacks within the equatorial ocean recharge oscillator model for ENSO, *Geophys. Res. Lett.*, *26*, 2989–2992.

Jin, F.-F., S.-I. An, A. Timmermann, and J. Zhao (2003), Strong El Niño events and nonlinear dynamical heating, *Geophys. Res. Lett.*, *30*, 1120, doi:10.1029/2002GL016356.

Karamperidou, C., M. A. Cane, U. Lall, and A. T. Wittenberg (2014), Intrinsic modulation of ENSO predictability viewed through a local Lyapunov lens. *Clim.e Dyn.*, 42, 253-270. doi: 10.1007/s00382-013-1759-z.

Kirtman, B. P. (1997), Oceanic Rossby wave dynamics and the ENSO period in a coupled model, *J. Clim.*, 10, 1690-1704.

Kug, J.-S., J. Choi, S.-I. An, F.-F. Jin, and A. T. Wittenberg (2010), Warm pool and cold tongue El Niño events as simulated by the GFDL CM2.1 coupled GCM, *J. Clim.*, *23*, 1226-1239. doi: 10.1175/2009JCLI3293.1.

Larson, S., S.-K. Lee, C. Wang, E.-S. Chung, and D. Enfield (2012), Impacts of non-canonical El Nino patterns on Atlantic hurricane activity. *Geophys. Res. Lett.*, *39*, L14706, doi:10.1029/2012GL052595.

Larson, S., and B. P. Kirtman (2014), The Pacific meridional mode as an ENSO precursor and predictor in the North American Multimodel Ensemble. *J. Clim.*, *27*, 7018–7032.

Lengaigne, M., J. P. Boulanger, C. Menkes, and H. Spencer (2006), Influence of the seasonal cycle on the termination of El Niño events in a coupled general circulation model, *J. Clim.*, *19*, 1850-1868.

Lengaigne, M., and G. A. Vecchi (2009), Contrasting the termination of moderate and extreme El Niño events in Coupled General Circulation Models, *Clim. Dyn.*, *35*, 299–313.

Lee, S.-K., R. Atlas, D. B. Enfield, C. Wang and H. Liu (2013), Is there an optimal ENSO pattern that enhances large-scale atmospheric processes conducive to major tornado outbreaks in the U.S.?, *J. Clim.*, *26*, 1626-1642.

Lee, S.-K., B. E. Mapes, C. Wang, D. B. Enfield and S. J. Weaver (2014), Springtime ENSO phase evolution and its relation to rainfall in the continental U.S., *Geophys. Res. Lett.*, *41*, 1673-1680.

Lim, E.-P., H. H. Hendon, D. Hudson, G. Wang, and O. Alves (2009), Dynamical forecast of inter El-Niño variations of tropical SST and Australian spring rainfall. *Mon. Wea. Rev.*, *137*, 3796-3810.

Lopez, H., and B. P. Kirtman (2014), Tropical Pacific internal atmospheric dynamics and resolution in a coupled GCM, *Clim. Dyn.*, doi 10.1007/s00382-014-2220-7.

McGregor, S., N. Ramesh, P. Spence, M. H. England, M. J. McPhaden, and A. Santoso (2013), Meridional movement of wind anomalies during ENSO events and their role in event termination, *Geophys. Res. Lett.*, *40*, 749–754, doi:10.1002/grl.50136.

McPhaden, M. J., and X. Zhang (2009), Asymmetry in zonal phase propagation of ENSO sea surface temperature anomalies, *Geophys. Res. Lett.*, *36*, L13703, doi:10.1029/2009GL038774.

Neelin, J. D. (1991), The slow sea surface temperature mode and the fast-wave limit: Analytic theory for tropical interannual oscillations and experiments in a hybrid coupled model, *J. Atmos. Sci.*, *48*, 584-606.

Ogata, T., S.-P. Xie, A. Wittenberg, and D.-Z. Sun (2013), Interdecadal amplitude modulation of El Niño/Southern Oscillation and its impacts on tropical Pacific decadal variability, *J. Clim.*, *26*, 7280-7297. doi: 10.1175/JCLI-D-12-00415.1.

Rasmusson, E. M., and T. H. Carpenter (1982), Variations in tropical sea surface temperature and surface wind fields associated with the Southern Oscillation/El Niño, *Mon. Wea. Rev.*, *110*, 354-384.

Smith, T. M., R. W. Reynolds, T. C. Peterson, and J. Lawrimore (2008), Improvements to NOAA's historical merged land-ocean surface temperature analysis (1880-2006), *J. Clim*., *21*, 2283-2296.

Takahashi, K., A. Montecinos, K. Goubanova, and B. Dewitte (2011), ENSO regimes: Reinterpreting the canonical and Modoki El Niño, *Geophys. Res. Lett*., 38, L10704, doi:10.1029/2011GL047364.

Trenberth, K. E., and D. P. Stepaniak (2001), Indices of El Niño evolution, *J. Clim., 14*, 1697–1701.

Vecchi, G. A. (2006), The termination of the 1997–98 El Niño. Part II: Mechanisms of atmospheric change, *J. Clim*., *19*, 2647–2664.

Vecchi, G. A., and D. E. Harrison (2006), The termination of the 1997–98 El Niño. Part I: Mechanisms of oceanic change, *J. Clim.*, *19*, 2633–2646.

Vecchi, G. A., A. T. Wittenberg, and A. Rosati (2006), Reassessing the role of stochastic forcing in the 1997-8 El Niño, *Geophys. Res. Lett., 33*, L01706. doi: 10.1029/2005GL024738

Vecchi, G. A., and A. T. Wittenberg (2010), El Niño and our future climate: Where do we stand? *Wiley Interdisciplinary Reviews: Climate Change*, 1, 260-270. doi: 10.1002/wcc.33.

Vimont, D. J., D. S. Battisti, and A. C. Hirst (2001), Footprinting: a seasonal link between the mid-latitudes and tropics, *Geophys. Res. Lett*., *28,* 3923–3926.

Wang, C., and R. H. Weisberg (1994), On the "Slow Mode" mechanism in ENSO-related coupled ocean–atmosphere models. *J. Clim*., 7, 1657–1667.

Wang, C., and X. Wang (2013), Classifying El Niño Modoki I and II by different impacts on rainfall in southern China and typhoon tracks. *J. Clim*., 26, 1322–1338.

Wittenberg, A. T. (2009), Are historical records sufficient to constrain ENSO simulations?, *Geophys. Res. Lett.*, *36*, L12702. doi: 10.1029/2009GL038710.

Wittenberg, A. T., A. Rosati, T. L. Delworth, G. A. Vecchi, and F. Zeng (2014), ENSO modulation: Is it decadally predictable?, *J. Clim.*, *27*, 2667-2681. doi: 10.1175/JCLI-D-13-00577.1.

Wu, R. and B. Wang (2002), A contrast of the East Asian Summer monsoon-ENSO relationship between 1962-77 and 1978-93, *J. Clim.*, *15*, 3266-3279.

Yeh, S.-W., J.-S. Kug, B. Dewitte, M.-H. Kwon, B. Kirtman, and F.-F. Jin (2009), El Niño in a changing climate, *Nature*, *461*, 511–514.

Yeh, S.-W., J.-S. Kug, and S.-I. An (2014), Recent progress on two types of El Niño: Observations, dynamics, and future changes, *Asia-Pac. J. Atmos. Sci*. *50*, 69-81.

Yu, J.-Y., H.-Y. Kao, and T. Lee (2010), Subtropics-related interannual sea surface temperature variability in the central equatorial Pacific, *J. Clim.*, *23*, 2869–2884.

Yu, J.-Y., and S. T. Kim (2010), Three evolution patterns of Central-Pacific El Niño, *Geophys. Res. Lett*., *37*, L08706, doi:10.1029/2010GL042810.

Zhang, H., A. Clement, and P. DiNezio (2014), The South Pacific meridional mode: A mechanism for ENSO-like variability, *J. Clim.*, *27*, 769–783.

Figure 1. Time-longitude plots of (a) CM and (b and c) the two leading inter-event EOFs of the tropical Pacific SSTAs averaged between 5°S and 5°N, for 21 El Niños during 1949–2013. (d and e) Same as b and c except that the two EOFs are rotated by 90º. Units are in ºC. The dashed gray boxes indicate Niño 3.4 in DJF (0,+1), Niño 3 (150°W–90°W and 5°S–5°N) in AMJ (+1), Niño 3 in AMJ (0), and Niño 3.4 in OND (+1).

Figure 2. Time-longitude plots of the equatorial Pacific SST (color shade), D20 (contour) and wind stress (vector) anomalies averaged between 5°S and 5°N, for (a) CM, (b) CM+EOF1, (c) CM-EOF1, (d) CM+EOF2, and (e) CM-EOF2 of the 21 El Niños during 1949–2013. The units are ºC for SST, m for D20 and dyne cm^{-2} for wind stress. The contour interval for D20 is 4.0 m. The longest wind stress vector corresponds to 0.34 dyne cm^{-2}.

Figure 3. (a) Normalized PC1 versus PC2 and (b) PC1+PC2 versus PC2-PC1 for all 21 El Niño events. The two digit numbers indicate the El Niño onset years.

Figure 4. Same as Figure 2 except for (a) CM, (b) CM+REOF1, (c) CM-REOF1, (d) CM+REOF2, and (e) CM-REOF2 of the 21 El Niños during 1949–2013.

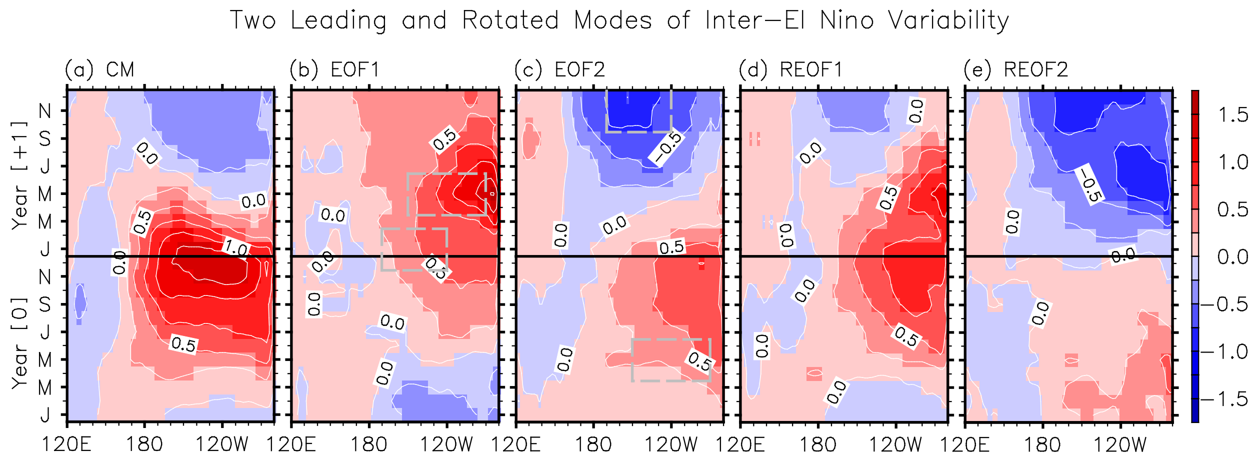

Figure 1. Time-longitude plots of (a) CM and (b and c) the two leading inter-event EOFs of the tropical Pacific SSTAs averaged between 5°S and 5°N, for 21 El Niños during 1949–2013. (d and e) Same as b and c except that the two EOFs are rotated by 90º. Units are in ºC. The dashed gray boxes indicate Niño 3.4 in DJF (0,+1), Niño 3 (150°W–90°W and 5°S–5°N) in AMJ (+1), Niño 3 in AMJ (0), and Niño 3.4 in OND (+1).

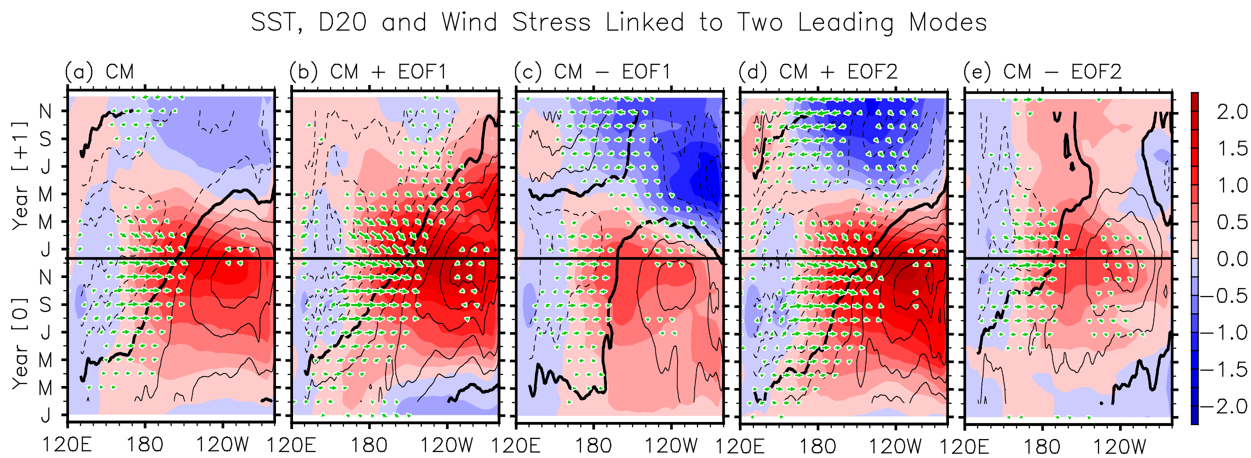

Figure 2. Time-longitude plots of the equatorial Pacific SST (color shade), D20 (contour) and wind stress (vector) anomalies averaged between 5°S and 5°N, for (a) CM, (b) CM+EOF1, (c) CM-EOF1, (d) CM+EOF2, and (e) CM-EOF2 of the 21 El Niños during 1949–2013. The units are ºC for SST, m for D20 and dyne cm^{-2} for wind stress. The contour interval for D20 is 4.0 m. The longest wind stress vector corresponds to 0.34 dyne cm^{-2}.

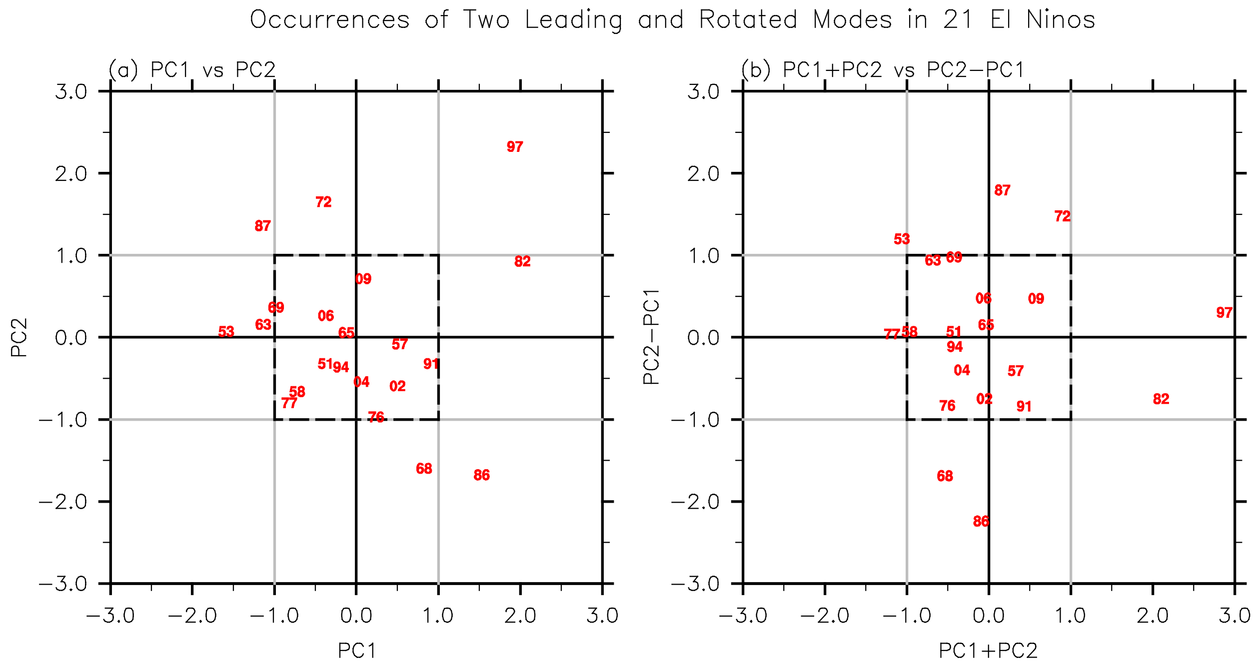

Figure 3. (a) Normalized PC1 versus PC2 and (b) PC1+PC2 versus PC2-PC1 for all 21 El Niño events. The two digit numbers indicate the El Niño onset years.

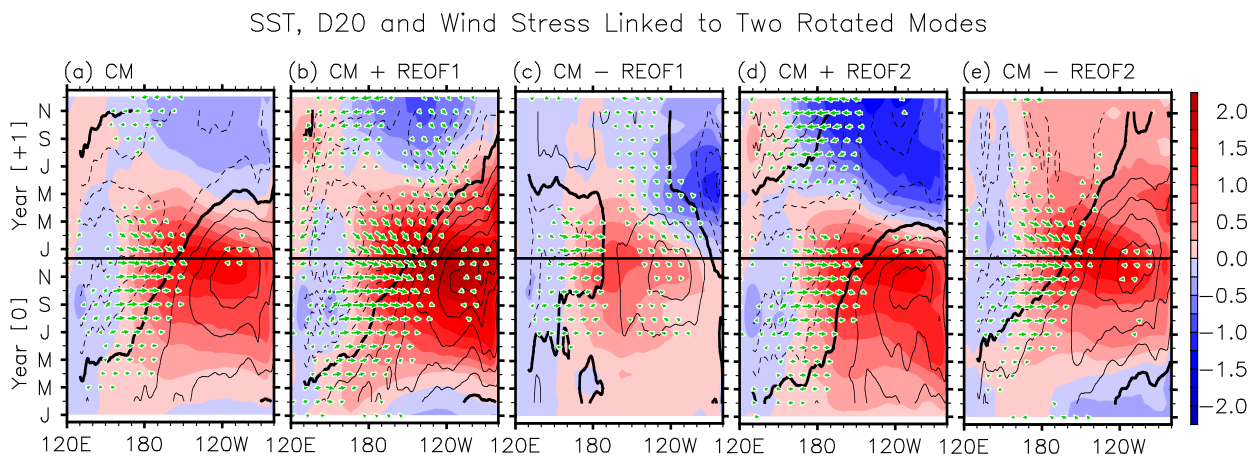

Figure 4. Same as Figure 2 except for (a) CM, (b) CM+REOF1, (c) CM-REOF1, (d) CM+REOF2, and (e) CM-REOF2 of the 21 El Niños during 1949–2013.